01 Sep 2023

In Situ Monitoring Of The Hydration Of Calcium Silicate Minerals In Cement With A Remote Fiber-optic Raman Probe

Bohong Zhang

Wenyu Liao
Missouri University of Science and Technology, wliao@mst.edu

Hongyan Ma
Missouri University of Science and Technology, mahon@mst.edu

Jie Huang
Missouri University of Science and Technology, jieh@mst.edu

Recommended Citation

B. Zhang et al., "In Situ Monitoring Of The Hydration Of Calcium Silicate Minerals In Cement With A Remote Fiber-optic Raman Probe," *Cement and Concrete Composites*, vol. 142, article no. 105214, Elsevier, Sep 2023.
The definitive version is available at https://doi.org/10.1016/j.cemconcomp.2023.105214

Cement and Concrete Composites 142 (2023) 105214

Contents lists available at ScienceDirect

Cement and Concrete Composites

journal homepage: www.elsevier.com/locate/cemconcomp

In situ monitoring of the hydration of calcium silicate minerals in cement with a remote fiber-optic Raman probe

Bohong Zhang [a], Wenyu Liao [b,1], Hongyan Ma [b,*], Jie Huang [a,**]

[a] Department of Electrical and Computer Engineering, Missouri University of Science and Technology, Rolla, MO, 65409, USA
[b] Department of Civil, Architectural and Environmental Engineering, Missouri University of Science and Technology, Rolla, MO, 65409, USA

ARTICLE INFO

Keywords:
In situ Raman spectroscopy
Fiber-optic Raman probe
Real-time continuous monitoring
Hydration process
Dicalcium silicate (C_2S)
Tricalcium silicate (C_3S)

ABSTRACT

This study utilized a novel *in situ* fiber-optic Raman probe to continuously monitor the hydration progress of tricalcium silicate (C_3S) and dicalcium silicate (C_2S) without the need for sampling, from early hydration stage to later stages, and from fresh to hardened states of paste samples. By virtue of the remarkable ability of this technique in characterizing either dry or wet and crystalline or amorphous samples, the hydration processes of C_3S and C_2S pastes with different water-to-solid (w/s) ratios could be monitored from the start of the hydration reaction. The main hydration products, calcium silicate hydrate (C–S–H) and portlandite/calcium hydroxide (CH), have been successfully identified and continuously monitored for variations in their respective amounts *in situ*. The effect of w/s ratio on the hydration processes of C_3S and C_2S pastes was also considered. Meanwhile, the x-ray diffraction (XRD) and thermogravimetric analysis (TGA) results showed a great correlation with the *in situ* Raman test results about hydration products, which demonstrated the reliability of this technology. Moreover, the signal-to-noise ratio (SNR) of this Raman probe is significantly superior to existing technologies for *in situ* fiber-optic Raman spectroscopy. This remote fiber-optic Raman probe enables the use of Raman spectroscopy in future construction projects for on-site monitoring and evaluation of health conditions and performance of concrete structures.

1. Introduction

Hydration reactions of cement-based materials are of great significance to their mechanical properties and durability. Various technologies have been applied to study the hydration processes regarding reaction heat, chemical changes, or microstructures, such as isothermal calorimetry, x-ray diffraction (XRD), thermogravimetric analysis (TGA), nuclear magnetic resonance (NMR), scanning electron microscopy equipped with energy-dispersive x-ray spectroscopy (SEM-EDS), and Raman spectroscopy [1–3]. The Raman activity during the hydration of pure cement phases, white cement, and ordinary Portland cement has been reported as early as 1976 [4]. Compared with other test methods, Raman spectroscopy has advantages such as [5,6]: 1) simple sample preparation; 2) rapid testing; 3) superb ability in recognizing both crystalline and poorly-crystallized phases; and 4) optional quick mapping and capability to reveal the global structure evolution of materials when combined with confocal microscopy. Taking advantage of these merits, Raman spectroscopy has been proven to be a valuable tool for characterizing clinker phases and hydration products, including tricalcium silicate (C_3S) [7], dicalcium silicate (C_2S) [8], tricalcium aluminate (C_3A) [9–11], tetracalcium aluminoferrite (C_4AF) [9,10], gypsum ($CaSO_4{\cdot}2H_2O$) [12], calcium hydroxide (CH) [13], calcium silicate hydrate (C–S–H) gel [14,15], ettringite (AFt) [16], and monosulfate (AFm) phases [4,9,17].

However, most of the existing Raman-powered studies on chemical changes used powder samples, and only a small number of *in situ* and real-time Raman tests on cementitious materials have been carried out. To enable *in situ* and/or real-time Raman tests, Tarrida et al. [7] cast C_3S paste (with a water-to-solid ratio, i.e., w/s ratio, of 0.4) in the glass tubes and examined the hydration kinetics of C_3S paste from 1 to 50 days via *in situ* unpolarized macro-Raman spectra, using a multichannel Raman spectrophotometer from Dilor was employed, which utilized a 514.5 nm green line of an ionized argon laser for excitation. In another study conducted by Black et al. [9], wet cementitious samples (with a high w/s

* Corresponding author.
** Corresponding author.
E-mail addresses: mahon@mst.edu (H. Ma), jieh@mst.edu (J. Huang).
[1] This author contributed equally to the first author.

https://doi.org/10.1016/j.cemconcomp.2023.105214
Received 2 March 2023; Received in revised form 4 July 2023; Accepted 18 July 2023
Available online 19 July 2023

ratio of 1.0) under glass coverslips were prepared. The *in situ* and real-time analyses of the hydrating C_3A and C_4AF pastes in the presence and absence of sulfate was performed with a Renishaw system 2000 Raman spectrometer fitted with a 632.8 nm (25 mW) He–Ne laser. In addition, Masmoudi et al. [18] implemented *in situ* Raman studies on the hydration process of cement paste with or without partial replacement of cement by volcanic ash from the fresh state at 10 min to the hardened state at 48 h. The cement paste samples (with a water-to-cement ratio, i.e., w/c ratio, of 0.55) were cast on a glass slide and measured by a Renishaw via Raman Microscope with an excitation wavelength of 785 nm line of a diode laser with an exposure time of 10 s and a grating of 1200 L/mm connected to a CCD camera detector. Moreover, Torres-Carrasco et al. [19] obtained *in situ* Raman spectra and images over a cement paste sample (w/c ratio of 0.35), revealing its hydration kinetics from the fresh state at 2 h to the hardened state at 48 h by confocal Raman microscopy (CRM). The CRM used a 5 mW laser power of a 532 nm excitation laser (green laser) and a 100 × oil objective lens (N.A. 1.25). As can be seen from the above studies, various wavelengths of lasers or/and different customized techniques have been used in cementitious materials inspection, aiming to obtain better *in situ* and real-time Raman spectra. The main reason for changing lasers in different wavelengths is that some fluorescent impurities in the analyzed cementitious samples can generate a strong fluorescent signal under specific wavelength lasers and thus interfere with the Raman spectra. Since the Raman spectra are calculated based on the energy difference between incident and scattered light, the Raman effect is independent of the laser wavelength. Hence, changing the wavelength of the laser source can effectively attenuate the excitation of fluorescent impurities in the sample to reduce the influence of the Raman fluorescence background signal without influencing the Raman effect. Regarding the techniques used in the above literature review, it can be noted that existing *in situ* and real-time Raman spectroscopy tests are usually carried out by bench-mounted Raman spectroscope in a laboratory condition and require some preparations for test samples, such as sampling, polishing, stoppage of hydration, or/and freeze/vacuum/oven drying. These facts limit the application of Raman spectroscopy for on-site real-time research and structure health monitoring (SHM). In addition to *in situ* Raman technology, previous studies have extensively investigated the monitoring of cementitious materials using various *in situ* methods, with a particular emphasis on the piezoelectric-based electromechanical impedance (EMI) approach [20–22]. These studies have primarily concentrated on the non-destructive monitoring of both the hydration process and the bond development occurring at the steel-concrete interface in reinforced concrete structures.

In recent years, optical fiber technology has experienced significant advancements [23–26], and fiber-optic Raman spectroscopy has burgeoned by integrating the transmission ability of optical fiber into the fingerprint characterization capacity of Raman spectroscopy systems, providing great potential for on-site real-time monitoring [27–33]. However, fiber-optic Raman spectroscopy has rarely been utilized to investigate the complex chemical reactions in cementitious materials. Several feasibility studies of using it on cementitious materials were performed by Yue et al. [34–38]. They had developed an optical fiber excitation Raman spectroscopy system using an "optical fiber excitation + spectrometer objective collection" configuration. Their research proved the viability of establishing and utilizing fiber-optic Raman spectroscopy for early hydration of cement paste at the fresh stage [38] and exploration of some durability-related mechanisms, such as chloride penetration, sulfate attack, and carbonation in cementitious materials [34–37]. However, the current optical fiber excitation Raman spectroscopy system relies on optical fibers solely for sample excitation, while signal collection and analysis are performed using a separate commercial benchtop Raman spectroscopy system. This dual setup increases the complexity of the testing system, making it more cumbersome and suitable mainly for laboratory use. Furthermore, in comparison to the original benchtop Raman spectroscopy system, the utilization of the optical fiber setup allowed for the examination of the sample's surface at the micron-scale under ambient conditions, regardless of the analyte states. However, this led to a significant reduction in the signal level. The reduced signal-to-noise ratio (SNR) of the Raman spectrum was primarily attributed to the lower excitation power density and signal collection efficiency of the fiber-optic setup. Consequently, this resulted in lower quality spectra and extended data collection times. Additionally, due to the reliance on the benchtop Raman instrument for signal collection, the fiber-optic system was unable to perform *in situ* inspections. Therefore, there is a pressing need for technical advancements in remote and *in situ* fiber-optic Raman spectroscopy systems. These advancements would facilitate the study of cementitious materials and enable the deployment of efficient, reliable, and real-time analysis techniques for in-field applications.

This paper presents an innovative approach using a remote fiber-optic Raman probe for *in situ* and real-time monitoring of early-/later-stage hydration of clinker phases, specifically C_3S and C_2S, in cementitious materials. Significantly, the fiber-optic Raman probe allows the rapid *in situ* and real-time monitoring of wet and dry cementitious samples via direct sample surface scanning without sampling and external interference. This study reveals the hydration processes of C_3S and C_2S from the early to later hydration stages following the evolution of C–S–H gel and CH. For data validation of the fiber-optic Raman probe, the spectrum of silica wafer was first acquired by the Raman probe and compared with that from commercial benchtop Raman spectroscopy. In addition, the XRD and TGA analyses were also conducted to verify the information obtained from the fiber-optic Raman probe. Based on the results harvested, the feasibility and potential of the fiber-optic Raman probe as an on-site and remote characterization and monitoring technique for cement hydration can be evaluated. The results projected that this fiber-optic Raman probe has great potential to become a novel sensor system to monitor the condition of concrete structures. Furthermore, it contributes to the advancement of remote1 monitoring of the hydration process of concrete in extreme environments, such as when concrete is utilized to immobilize radioactive waste in nuclear facilities and many other applications.

2. Materials and methods

2.1. Sample preparation

The C_3S and C_2S materials used in this research were purchased from Kunshan Chinese Technology New Materials Co., Ltd. (Jiangsu, China). Their purities were both higher than 99%. De-ion water was used in the preparation of all samples. C_3S pastes with two different w/s ratios (i.e., 0.4 and 0.5) and C_2S pastes with three different w/s ratios (i.e., 0.5, 0.55, and 0.6) were prepared and cast in 2 × 2 × 2 cm cube molds for the testing. In the realm of cement research, different w/s ratios are commonly employed for C_3S and C_2S due to their distinctive reactivity and hydration characteristics. The w/s ratio plays a crucial role in determining the availability of water for hydration reactions and significantly influences the hydration process of each compound. C_3S, being the most reactive compound in cement, plays a vital role in the early-age strength development. It readily reacts with water, resulting in the formation of calcium silicate hydrates (C–S–H), which contribute to the binding and strength of the cementitious matrix. Optimal hydration of C_3S requires a w/s ratio between 0.4 and 0.5, providing sufficient water for dissolution, hydration, and the formation of hydration products that enhance the strength and durability of the cementitious matrix. Additionally, a w/s ratio of 0.4–0.5 facilitates the development of a workable paste with favorable flowability. This ensures that the cementitious mixture can be easily mixed, placed, and consolidated during construction or testing processes. Consequently, w/s ratios of 0.4 and 0.5 are chosen for preparing C_3S samples in order to investigate them further.

A w/s ratio of 0.5 is commonly employed for C_2S as it provides a

well-balanced amount of water for hydration, ensuring reasonable reactivity and achieving a satisfactory compromise between workability and strength development of the cement paste. A slightly higher w/s ratio of 0.55 is selected to explore the influence of increased water availability. This ratio facilitates a greater water supply, enhancing the hydration process and potentially leading to higher hydration degree and improved strength development. The objective is to investigate the effect of increased water content on the kinetics of hydration and the resulting properties of the cementitious material. Furthermore, a w/s ratio of 0.6 is chosen to increase the water content in the mixture further. This promotes more extensive hydration of C_2S and can significantly influence the microstructure and properties of the cementitious system.

2.2. Raman spectroscopy, XRD, and TGA

In Raman spectroscopy analysis, a chemical component is identified by its characteristic peak, known as Raman shift [39]. The Raman shift is unique for each component due to the unique molecular vibrations that exist within this component. Therefore, the chemical composition in a sample can be determined by analyzing the Raman shift. By studying the hydration process of cementitious powders, the Raman shifts can be determined. For example, C_3S has a strong vibration corresponding to a broad frequency shift from 813 to 890 cm^{-1}, but the most intensive peaks are located from 840 to 848 cm^{-1} [40–43]. A substance may have more than one designated Raman shift. For C–S–H Raman spectra, it has two designated regions of characteristic shifts caused by the vibration of two different types of comparable molecular solids in these two regions [40,41,43]. The peak at 600 to 700 cm^{-1} is caused by the Si–O–Si bending mode in C–S–H gels, while the peak at 520 to 550 cm^{-1} corresponds to the $\nu 4$ internal modes of the SiO_4^{4-} chemical bond [40–43]. In summary, the Raman peaks of the leading chemical substances involved in this study are listed in Table 1.

The XRD analysis was carried out to verify the phases change of the hydration process of C_3S and C_2S pastes. The hydration reactions of paste samples were stopped by immersing initially crushed paste in high-purity isopropanol for 24 h. Then, the paste samples were dried in a vacuum desiccator and ground into powder for testing. The XRD tests were carried out by a PANanalytical X'pert Pro MPD diffractometer, using CuKα radiation ($\lambda = 1.54$ Å) and an X-Celerator solid detector. The diffraction patterns were examined with 2θ ranging from 10° to 65° and a scan speed of 0.03348°/s.

In addition, the TGA analysis was conducted to measure the weight change of C_3S and C_2S pastes as a function of temperature under controlled heating conditions. The main goal of utilizing TGA is to quantify the change of composition to further correlate with the Raman results. Prior to testing, the samples were collected at specific testing ages and subsequently ground into fine powders. A solvent exchange method was employed to halt the hydration process, involving immersing the samples in isopropanol for 15 min, followed by thorough rinsing with diethyl ether. The samples were then dried in a vacuum oven for 1 h to remove any residual solvents. The TGA method utilized in this research study involved heating the prepared samples from 30 °C to 1000 °C, at a heating rate of 10 °C/min. The tests were carried out under a nitrogen (N_2) atmosphere, maintaining a constant flow rate of 100 ml/min.

Table 1
Characteristic Raman peaks for cementitious ingredients and hydration products summarized from pioneering research.

Chemical ingredients	Raman shift (cm^{-1})
C_3S	834–845 [40–43]
C_2S	846–864, 972–975 [40–44]
CH	354–359 [40,41,43]
C–S–H	425–500, 600–700 [41,42,44]
$\nu_4[SiO_4^{4-}]$	520–550 [42,43]
$\nu_1[SiO_4^{2-}]$	979–984 [42,43]

3. Instrumentation

An *in situ* fiber-optic Raman probe was employed to study the chemical changes of C_3S and C_2S samples during the hydration process. The Raman probe was constructed with a probe body and an extension probe. A 105 μm core diameter fiber and a 100 μm core diameter fiber was employed inside the probe to work as the optical excitation and absorption path. A long-pass filter (OD 1) and a band-pass filter (centered at 532 nm) were installed inside the probe to block laser reflections and eliminate inelastic background signals generated by the silica fiber. A convex sapphire lens was employed at the probe's tip to provide a working distance of 7.5 mm for the Raman probe for noncontact measurement. In addition, a 25 cm long extended probe with a tip diameter of 0.9 cm was installed with the probe body for testing in small and harsh environments. A 532 nm laser (green laser) with 100 mW source power and a 3 cm^{-1} spectral resolution QE pro spectrometer were used in the Raman system. The laser spot size on the target sample is approximately 100 μm when the working distance is 7.5 mm. During the experiment, Raman spectra were collected with the QE-Pro spectrometer. The Raman spectra region was focused on between 100 and 1500 cm^{-1} which has the most significant chemical features of the cement paste material. The data acquisition time was set to 30 s with Oceanview software (Ocean Optics, Inc.). Furthermore, five Raman spectra were collected and averaged for each measurement to ensure a good SNR. All spectra were obtained with these stated experimental parameters. A vacuum chamber was used to ensure that the sample would not be over-carbonized during the experiment. Several hollow channels were made in the top of the vacuum chamber to allow for the installation of the Raman probe, vacuum pump, oxygen cylinder, CO_2 sensor, and pressure gauge. As shown in Fig. 1, a rubber tube was designed to seal the gap between the hollow channels and the insertion device. After the device cable and rubber tube were inserted, epoxy glue was used to seal the rest of the gap. A vacuum pump was inserted into the vacuum chamber to extract the air and clean the hydration cement materials' experimental environment. While pumping, an oxygen cylinder was used to supply oxygen to the vacuum chamber to balance the air pressure inside the chamber. An external pressure gauge was mounted above the vacuum chamber to monitor the pressure inside. In addition, saturated sodium chloride solution was placed in the vacuum chamber as a humidity control agent. In real-time, a humidity meter and a carbon dioxide sensor were used to detect the humidity value (~70%) and check the carbon dioxide level (<10 ppm) in the vacuum chamber. The samples are placed in the vacuum chamber immediately after being mixed. Once the vacuum chamber is closed, the test samples are subjected to a long-term and real-time Raman data acquisition period.

4. Results and discussion

4.1. In situ fiber-optic Raman probe calibration by the silicon wafer

A silicon wafer was employed as a calibration standard to assess the performance of the fiber-optic Raman system. The well-defined Raman peak of silicon at 520 cm^{-1} was used for calibration purposes. Fig. 2 illustrates the Raman spectrum of the silicon wafer obtained using the *in situ* fiber-optic Raman probe. The Raman signal from the silicon wafer was successfully retrieved and exhibited excellent agreement with the expected sharp peak at 520 cm^{-1}, as previously reported in the literature [37,45]. This outcome strongly indicates the reliability and accuracy of the characterization results achieved by the proposed fiber-optic Raman system. Additionally, the results obtained from this study demonstrate a significantly improved SNR compared to previous investigations in the field [34–37]. The observed improvement in the SNR can be ascribed to a combination of key factors incorporated into the experimental setup. In order to mitigate the interference signal originating from the silica

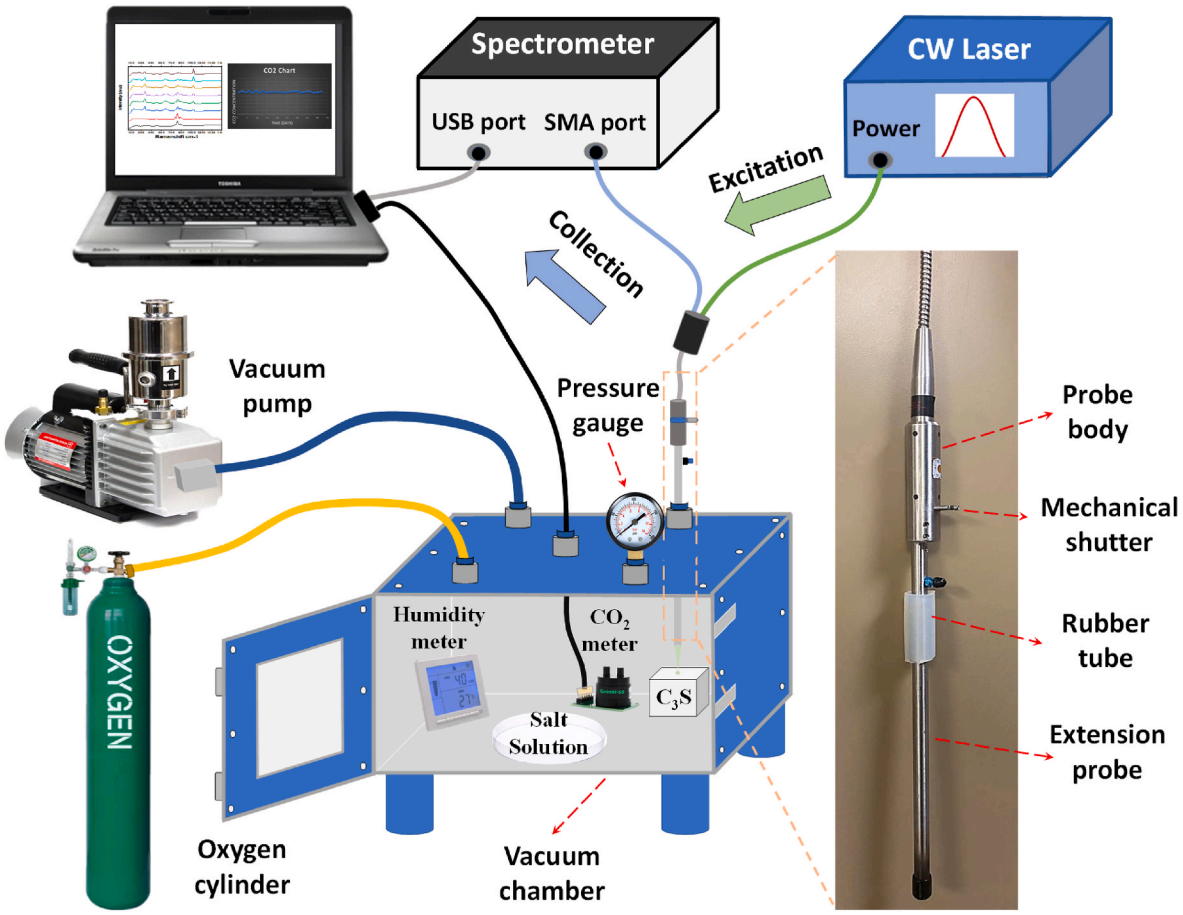

Fig. 1. The schematic diagram of the *in situ* fiber-optic Raman probe in experiment. The Raman probe was inserted into the vacuum chamber for continuous measurement. A 0.75 cm working distance was provided between the probe tip to the testing sample. The air inside of the vacuum chamber was evacuated by a vacuum pump.

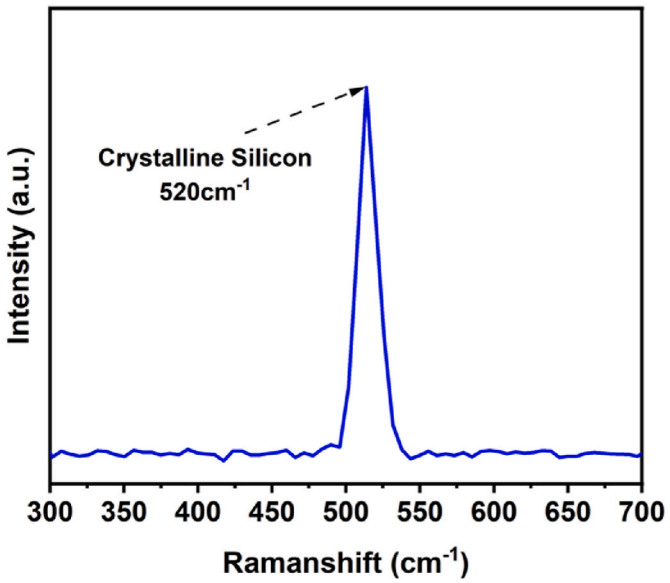

Fig. 2. Raman spectra of silicon wafer collected from the *in situ* fiber-optic Raman probe. A sharp Raman peak was observed at 520 cm^{-1}. (For interpretation of the references to colour in this figure legend, the reader is referred to the Web version of this article.)

fiber, a dual optical fiber configuration was implemented. This arrangement effectively eliminated the interference signal by employing two optical fibers into the fiber-optic Raman probe, ensuring a clean and accurate measurement of the Raman spectra discussed in our previous study [31,33]. To enhance the excitation efficiency and optimize photon delivery to the target samples, convex lenses were strategically introduced at the distal end of the fiber-optic Raman probe. These convex lenses facilitated the precise focusing of incident light onto the sample surface, generating a higher density of excited photons and significantly improving the overall excitation efficiency. The integration of convex lenses within the probe design enhanced the photon flux, leading to improved Raman signal acquisition and heightened sensitivity for accurate measurements. Additionally, in order to reduce the interference caused by laser reflection, optical filters were meticulously incorporated into the probe assembly. These optical filters were strategically positioned to filter out the laser reflection signal selectively, thereby diminishing unwanted background signals and minimizing interference.

4.2. C_3S hydration reaction monitored by in situ fiber-optic Raman probe

With the previous description of the *in situ* fiber-optic Raman system, this section will focus on the results and discussion of the experiments. To reflect the effect of water content on the hydration products and the reaction time, two C_3S pastes with w/s ratios of 0.4 and 0.5 were prepared, respectively. The two prepared samples were separately placed in a vacuum chamber for 60 days to monitor the cement hydration reaction. The pressure, humidity, and CO_2 concentration in the vacuum chamber during the hydration reaction were accurately controlled. Due

to the time expense in preparing the samples and providing the experimental environment, the Raman spectra collection started after 5 min of hydration of the C_3S. In order to ensure the high SNR of Raman spectra, all Raman spectra were taken with an integration time of 30 s and a 5-fold average. During the first 24 h of the hydration process, the Raman spectra were taken every 30 min using the in-house programmed software. After 24 h of hydration, the interval of spectrum acquisition was adjusted to be 2 h. The *in situ* real-time Raman spectra were analyzed from 5 min at the beginning of hydration to 60 days at the end of hydration, and the Raman region was from 300 to 1200 cm^{-1}, which included the most significant features of the hydrated C_3S paste samples, as shown in Fig. 3. Fig. 3 (a) & (b) show the Raman spectra of C_3S paste samples with 0.5 and 0.4 w/s ratios. Both Fig. 3 (a) and (b) reveal three distinct Raman peaks centered at around 842 cm^{-1}, representing the raw material component of C_3S [40–43], which are the most evident on the spectra collected 5 min after the material has been hydrated. At 526 cm^{-1}, a Raman peak with relatively low Raman intensity was found from both w/s ratio samples, corresponding to the $\nu 4$ internal modes of the SiO_4^{4-} chemical bond [42,43]. This Raman peak also explains the presence of silica in the C_3S paste material. The main products of C_3S hydration, i.e., CH and C–S–H, were not found in the Raman spectra during the first 5 min of the C_3S hydration for both w/s ratio samples. At

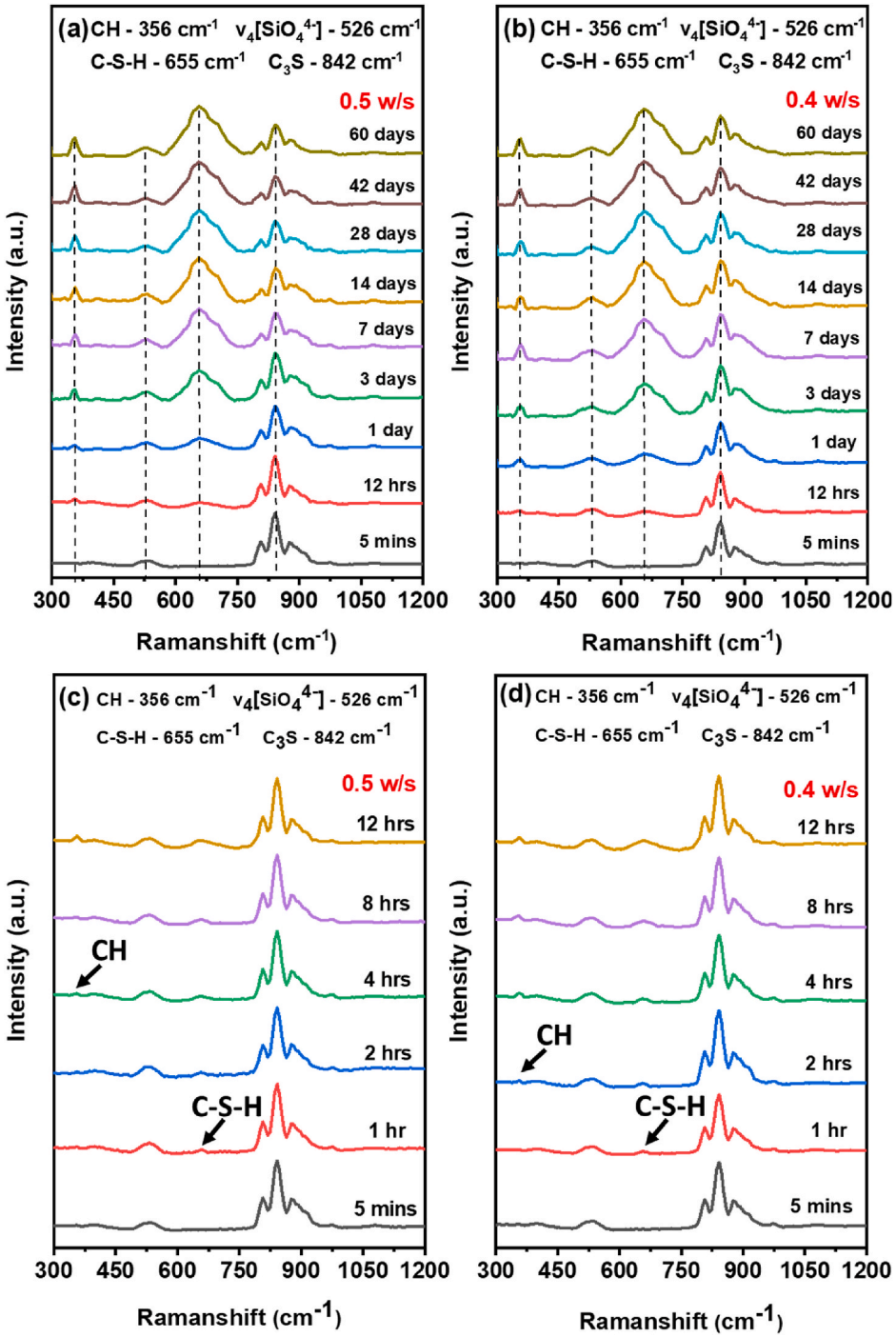

Fig. 3. Raman Spectra of C_3S hydration samples with varying w/s ratios from 5 min to 60 days. (a) Raman spectra of 0.5 w/s C_3S sample hydration reaction in 60 days. (b) Raman spectra from 0.4 w/s C_3S sample hydration reaction in 60 days. (c) Raman spectra of 0.5 w/s C_3S sample hydration reaction from 5 min to 12 h. (d) Raman spectra of 0.4 w/s C_3S sample hydration reaction from 5 min to 12 h.

12 h of the C_3S hydration, the spectrum was still dominated by the three Raman peaks centered at 842 cm^{-1}, but a slight change was observed in the 500–700 cm^{-1} Raman region. The hydration reaction did not affect the $\nu 4$ internal modes of the SiO_4^{4-} chemical bond at 526 cm^{-1} after 12 h of hydration. However, a weak Raman peak at 655 cm^{-1} could be found in the Raman spectra. After comparing and analyzing the results with those of previous studies, it can be concluded that this Raman peak at 655 cm^{-1} belongs to C–S–H [40,41,43]. However, comparing the Raman spectra of C_3S pastes with 0.4 and 0.5 w/s ratios within the first 12 h of hydration, as shown in Fig. 3 (c) & (d), a peak at 356 cm^{-1} was observed to be a little more significant with the 0.4 w/s C_3S sample. Additionally, the CH was observed with 0.4 w/s at 2 h, but with 0.5 w/s between 2 and 4 h, which indicates a relatively later formation detectable of CH in pastes with higher w/s ratios. This result demonstrated that the C_3S paste with a higher w/s ratio might undergo a longer dormant period, which causes the later hydration and delayed formation of CH [40,41,43]. By comparing the Raman spectra of both 0.4 and 0.5 w/s C_3S hydration samples for one and three days, it is clearly demonstrated that the relative Raman spectra of the hydration products C–S–H and CH become more and more intense as the hydration reaction proceeds. After three days of the hydration reaction, the Raman peaks of the original reactants C_3S could be seen to become weaker gradually, while the Raman peaks of the products C–S–H and CH continually increased. This phenomenon was verified in both samples with different w/s ratios. At the final stage of the hydration reaction (60 days), both hydration ratios of the samples exhibit the characteristic peaks of CH, $\nu_4[SiO_4^{4-}]$, C–S–H, and C_3S. After a long hydration period, the product C–S–H replaces the reactant C_3S to become dominant in the Raman spectrum for the 300–1200 cm^{-1} Raman region.

As discussed, Raman spectroscopy is well known as an excellent qualitative detection tool for detecting the decrease or disappearance of cement clinker minerals and the appearance of hydration products. However, the quantitative analysis of samples by Raman spectroscopy has always been a subject of research significance and a great challenge. From the previous studies and the results of this paper, it can be seen that the main products of C_3S hydration are concentrated in the C–S–H at 655 cm^{-1}, while the dominant Raman peak of the C_3S hydration products is at 842 cm^{-1} [41–44]. Therefore, to further investigate the hydration process and chemical composition of C_3S with two different w/s ratios, the Raman region of 550–950 cm^{-1} was exemplified, as shown in Fig. 4.

In order to show more clearly the process of the C_3S hydration reaction, more sets of Raman data at different times are added to Fig. 4. Fig. 4 (a) and (b) show the Raman 3D plots of the C_3S hydration reaction at 0.5 and 0.4 w/s ratios, respectively. The intensity of the C–S–H Raman peak increases with the hydration reaction, and the C_3S Raman peak decreases with the hydration reaction, as seen from the Raman spectra presented in the 3D plots. As illustrated in Fig. 4, the Raman signal of the C–S–H product in both 0.4 and 0.5 w/s C_3S samples initiated the reaction at a similar time. However, at the 21-day mark, the Raman peak intensity of C–S–H in the 0.4 w/s sample exhibited almost no discernible growth trend, whereas the Raman peak intensity of C–S–H in the 0.5 w/s sample continued to exhibit a graduate increase. This observation suggests that the larger the w/s ratio of the C_3S paste sample, the longer the dormant period, aligning with our previous findings and the conclusions drawn in the referenced research [40,41]. At 42 days of the hydration reaction, the intensity of the C–S–H Raman peak of 0.5 w/s C_3S paste tends to slow down significantly, and there is almost no significant increase compared with the Raman peak of the C–S–H after 60 days of the hydration reaction. To better infer and demonstrate the hydration process of cement clinker by Raman spectroscopy, the Raman peak intensities of C–S–H at 655 cm^{-1} and C_3S at 842 cm^{-1} were extracted for a deeper analysis.

Raman spectroscopy provides valuable insights into molecular vibrations and structural changes within a material. It relies on the inelastic scattering of light, where incident photons interact with the sample, causing energy exchange with the molecular bonds. This interaction results in the emission of scattered light with different energy levels, which can be detected and analyzed. Different phases or components in a material can exhibit distinct Raman spectra due to molecular vibrations or crystal structure variations. As the hydration process progresses, phase transitions or transformations may occur, leading to changes in the material's composition and structure. These changes can manifest as alterations in bond lengths, bond strengths, and molecular interactions. These phase transitions can be accompanied by alterations in the Raman spectra, including changes in peak positions, intensities, or line widths. An increase in the intensity of a specific Raman peak suggests an enhancement or accumulation of the corresponding molecular species or phase. Since the fiber-optic Raman probe continuously monitors the cementitious sample *in situ* during the entire experiment without any external interference, the intensity of Raman peaks directly correlates to the corresponding vibrational mode population. Vibrational modes with higher populations will generate Raman signals with greater intensity. Therefore, continuous monitoring of the Raman spectra is beneficial to track the changes in peak intensities and correlate them with variations in the concentration of specific phases or molecular species. This information provides insights into the redistribution or enrichment of components during hydration. Additionally, to further differentiate between samples with different water ratios, the ratios of Raman peak intensities between the reactants and products

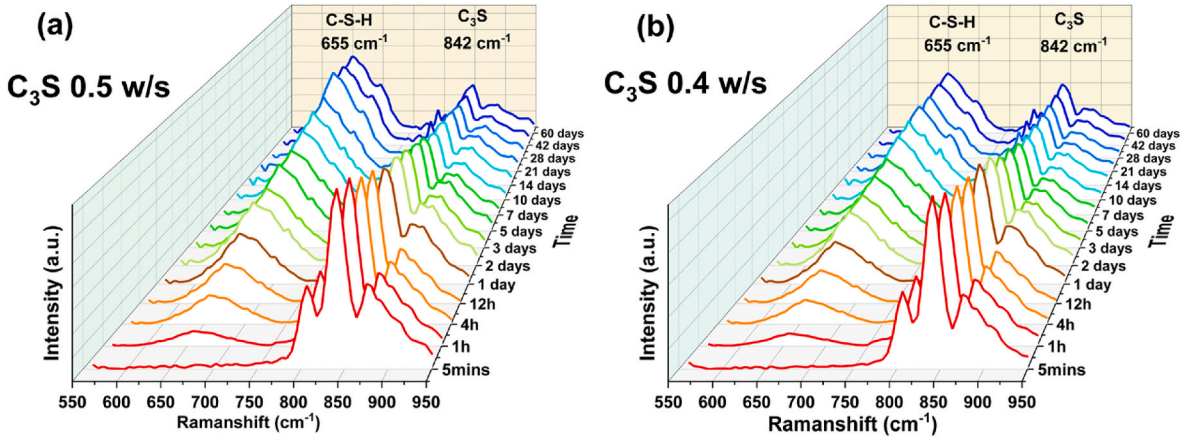

Fig. 4. The 3D Raman spectra of C_3S hydration samples with two different w/s ratios from 5 min to 60 days in the Raman region between 550 and 950 cm^{-1}. (a) 3D Raman spectra of the 0.5 w/s C_3S hydration sample. (b) 3D Raman spectra of the 0.4 w/s C_3S hydration sample. Two significant peaks of C–S–H and C_3S were observed at 655 and 842 cm^{-1} at both samples with w/s ratios of 0.4 and 0.5.

were investigated. This additional analysis provides a more accurate correlation for distinguishing between samples with varying water content. Therefore, the Raman peak intensity ratios of the reactants and products in the spectra were correlated with the hydration reaction time to further analyze the hydration reaction's mechanism, as shown in Fig. 5. When the hydration reaction proceeded for about 21 days, the 0.4 w/s C_3S sample first showed a flat growth curve, implying that it entered the final stage of the hydration reaction. The higher hydration ratio of 0.5 w/s sample showed a slow growth trend at about 28 days and entered the late stage of hydration reaction at day 42. This data reinforces the finding of longer hydration cycle for cement materials with higher w/s ratios.

There are several methods and models used to study and model the hydration process of cement. Kinetic models describe the dissolution of cement clinker and can be extended to capture later stages of hydration, providing a comprehensive view of the process [46]. Experimental methods, such as quantitative analysis and seawater testing, allow for the direct determination of composition and provide insights into the effects of environmental factors on cement hydration [47,48]. Thermodynamic modeling employs calculations to predict the formation and stability of cement hydrates, aiding in understanding phase evolution [49]. Researchers often combine these approaches to gain a deeper understanding of cement hydration and its impact on material properties. According to the observation in Fig. 5, the fitted growth patterns of the ratios of Raman peak intensities of the product (C–S–H) to the reactant (C_3S) are very much similar to the Avrami function model [50]. The Avrami equation essentially describes how a solid transform from one phase (state of matter) to another at a constant temperature [50–53]. It assumes the reaction can be complete and can be generally applied to investigate the chemical reaction rates of materials. However, the cement's hydration can never be completed in a cement paste's actual reaction. Due to this discrepancy between the assumptions of the Avrami equation and the nature of the hydrated cement, the experimental results of fitting the hydration kinetics with the Avrami equation usually need modification by introducing another parameter to make the fitting results better. The modified Avrami equation can be used to describe the hydration kinetics of cement in the form of

$$\alpha = -\alpha_u * e^{(-t)^n * k} + \alpha_u \quad (1)$$

where k and n are constants, α is the fraction of material reacted as a function of time, and α_u is newly introduced and assigned as the maximum/ultimate degree of hydration. In light of the modified Avrami equation for cement hydration and the similar fitting function models obtained in Fig. 5, the variations of C_3S peak intensities were called out for further analysis of C_3S consumption along with hydration time in Fig. 6 in order to understand better the relationship between Raman spectra of hydrated C_3S and degree of hydration reaction. The most dominant peak at 842 cm^{-1} in the C_3S Raman spectrum was used in this discussion. The Raman peak at 842 cm^{-1} at 5 min hydration was set as the initial value of zero while calculating the C_3S peak intensity variation. Compared with the Raman peak at the initial 5 min hydration, the consumption of Raman peak intensity was collected for different hydration periods, normalized, and fitted. However, after rigorous data analysis and literature review, it was found that the Avrami equation is commonly used as a model for early hydration reactions [52–54] and is not necessarily applicable to long-period hydration reactions. The degree of hydration would be varied along with the hydration reaction. Because of this reason, the following relation was unfolded for the normalized variations of C_3S peak intensities and the hydration reaction times, which is

$$\alpha = -\alpha_1 * e^{(-t)^n * k} + \alpha_1 * M \quad (2)$$

where α is normalized C_3S peak intensity variation (i.e., consumption, corresponding to the degree of reaction), k and n are constants, α_1 is a control parameter regarding the degree of reaction in the early hydration stage, and M is an adjustment parameter to better fit the long-period hydration stage. The C_3S peak intensity variation can somewhat reflect the C_3S consumption, and the above relation can reflect the hydration kinetics of C_3S and the degree of hydration from low to high. Based on Eq. (2), the 0.5 and 0.4 w/s C_3S hydration samples' Raman data can be fitted reasonably well, and a minimum R square value of 0.993 is obtained to address the curve fitting uncertainties. In Fig. 6, the Raman peak of the reactant C_3S at 842 cm^{-1} decreases gradually with the increase of the hydration reaction time. Both 0.5 and 0.4 w/s C_3S

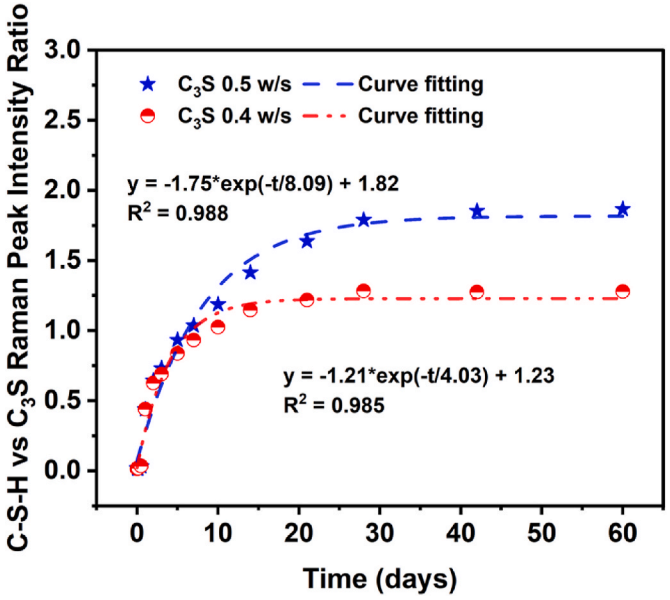

Fig. 5. The relative Raman peak ratio of C–S–H and C_3S as a function of time. The blue dot represents the 0.5 w/s C_3S hydration sample, and the red dot represents the 0.4 w/s C_3S hydration sample. Two exponential functions were applied for the curve fitting analysis. A minimum 0.985 R square value indicates the curve fitting accuracy. (For interpretation of the references to colour in this figure legend, the reader is referred to the Web version of this article.)

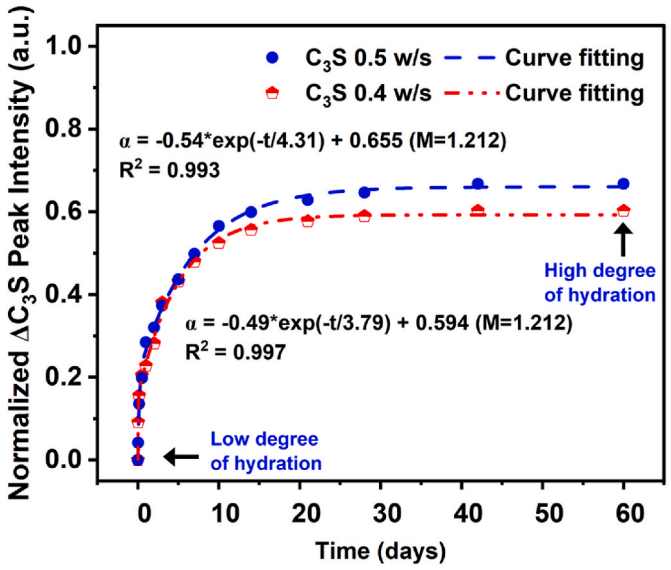

Fig. 6. The consumption (mirrored by variation of Raman peak intensity) of C_3S as a function of time. The blue dot represents the 0.5 w/s C_3S hydration sample, and the red dot represents the 0.4 w/s C_3S hydration sample. Two curve fitting functions between consumption of C_3S and time were discovered and mirrored the degree of hydration. (For interpretation of the references to colour in this figure legend, the reader is referred to the Web version of this article.)

hydration samples' signals show that the Raman peak intensity of C_3S at 842 cm^{-1} changes dramatically in the first ten days. Due to the less amount of water, the 0.4 w/s C_3S sample shows a slightly less steep curve than the 0.5 w/s C_3S sample at 14 days and becomes flattened at 28 days. The 0.5 w/s C_3S sample with a higher w/s ratio possesses a slower/delayed hydration kinetics at the initial stage due to its long dormant period. However, it has a faster hydration rate at 14 days and becomes flattened after 28 days with a higher C_3S consumption level, demonstrating a higher degree of hydration. Coefficient M was calculated as 1.212 for both 0.5 and 0.4 w/s C_3S samples, indicating the sustained reactivity of C_3S over time. This observation underscores the persistent nature of hydration reactions in C_3S, which contribute to the gradual development of cementitious properties and strength as the degree of hydration advances. By establishing the coefficient 'M' as 1.212 for both the 0.5 and 0.4 w/s C_3S samples, the research reinforces the understanding that C_3S exhibits a prolonged hydration behavior characterized by a continuous increase in the degree of hydration over an extended period. These findings have significant implications for the design and optimization of cementitious materials, providing a deeper comprehension of the hydration kinetics and performance of C_3S in various construction applications. Further investigation will be keep carrying on in the future research.

In order to validate the findings of the Raman spectroscopy analysis and determine the phases present in the cement paste, XRD analysis was conducted. Fig. 7 illustrates the XRD pattern results depicting the progression of hydration in the C_3S sample at various time intervals, including the initial state, 12 h, 14 days, 28 days, and 60 days. The XRD results reveal distinct features at different stages of hydration. In the raw state, the anhydrous mineral phase C_3S is clearly identified. As the hydration reaction proceeds, the formation of $Ca(OH)_2$ and C–S–H gel becomes apparent, as observed at the 12-h time point. During the period from 14 to 28 days, the intense peak corresponding to the raw C_3S phase diminishes significantly, indicating its consumption during the hydration process. At 60 days of hydration, the XRD pattern demonstrates a considerable presence of $Ca(OH)_2$ and a small amount of unreacted C_3S material. The observed decrease in the peaks associated with the C_3S feedstocks after 60 days of hydration aligns well with the Raman spectroscopic results discussed earlier, confirming the consumption of these silicates during the hydration process. The poorly ordered nature of C–S–H prevents its characterization as sharp peaks in the XRD pattern. However, its presence can be identified as a broad peak or a hump, indirectly verified by the consumption of calcium silicate C_3S. The XRD verification further substantiates the accuracy of Raman spectroscopy in elucidating the principles of the hydration reaction using a remote fiber-optic Raman probe. Consequently, the application of *in situ* real-time fiber-optic Raman sensors in the cement industry exhibits promising potential.

The TGA method can be used to determine the degree of hydration. It was observed that the decomposition of Portlandite occurs between approximately 370 °C and 500 °C. The tangential method was used to identify the onset and end points of this decomposition, allowing for the calculation of Portlandite content based on the weight loss attributed to the release of H_2O from Portlandite within the specified temperature range. Subsequently, the C–S–H gel content could be calculated using stoichiometric relations derived from the hydration reaction equations. Finally, the degree of hydration was determined by comparing the content of the hydrated product (C–S–H gel) to the unreacted cementitious materials. This comparison provided insights into the extent of cementitious material hydration. Based on the TGA curves displayed in Fig. 8, the degrees of hydration of the C_3S paste were determined and presented in Fig. 9. As depicted in the figure, the Raman and TGA results exhibit a generally consistent trend with slight discrepancies observed at certain ages. Several potential reasons account for the variation between the Raman and TGA results: Firstly, the Raman analysis examines a relatively smaller or different area compared to the TGA samples. In future tests, it is advisable to include duplicate samples to enhance the

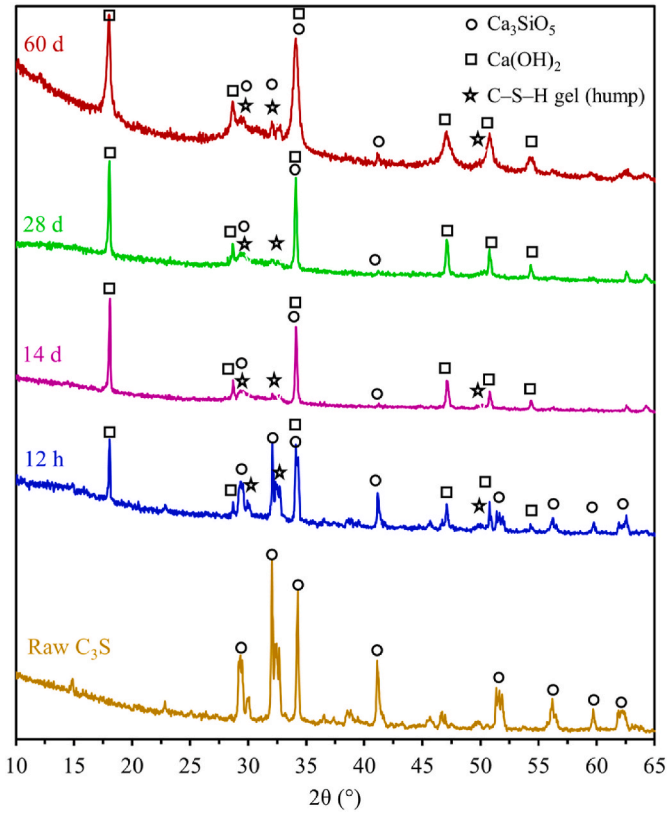

Fig. 7. XRD results of the hydration process of the C_3S sample. XRD patterns illustrate the hydration progress of the C_3S sample at different time intervals, including the raw state, 12 h, 14 days, 28 days, and 60 days.

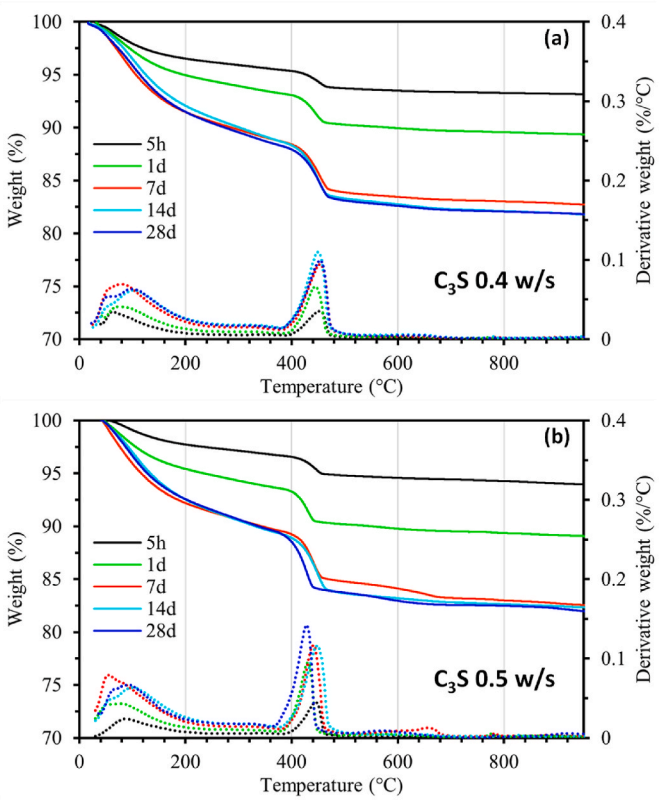

Fig. 8. TGA curves of C_3S paste samples with w/s ratio of 0.4 (a) and 0.5 (b).

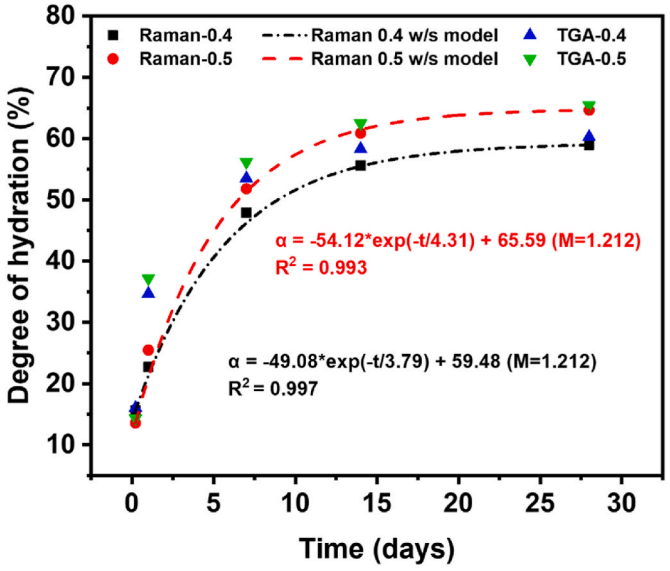

Fig. 9. Degrees of hydration of C_3S paste samples, in comparison with Raman results.

reliability and accuracy of the analysis, although the current study primarily focuses on evaluating the feasibility and potential of the technique. Secondly, the TGA method may introduce systematic or random measurement errors due to factors such as sampling and sample preparation, determination of onset points, procedural influences, method biases, and environmental effects such as carbonation during the test and sample handling. Lastly, interference from the water-rich surface layer has the potential to occur during the initial hydration phase of Raman probe testing. To address this issue, future investigations will explore the optimization of immersible fiber Raman sensors.

4.3. C_2S hydration reaction monitored by in situ fiber-optic Raman probe

C_3S and C_2S are essential components of silicate cement. They both have hydraulic properties and can react with water or aqueous solutions to produce hydrated calcium silicate (C–S–H) or/and (CH) as the main hydration product, thus contributing to the material's self-consolidation properties and spontaneous strength. However, the main difference between C_3S and C_2S comes from the chemical composition. From the perspective of their molecular weights, C_2S contains a higher calcium percentage than C_3S. Theoretically, when hydrating two samples of the same mass, C_2S will consume more water over hydration and have a higher amount of hydration products due to its higher calcium content. To examine this property, three samples of C_2S were prepared with different water ratios, 0.5, 0.55, and 0.6 w/s, respectively. The three C_2S samples were each placed in a vacuum chamber for 60 days for hydration reaction experiments. Real-time Raman spectra were collected 5 min after the start of the hydration reaction until 60 days of hydration, as shown in Fig. 10. Four dominant Raman peaks, C–S–H, $\nu_4[SiO_4^{4-}]$, and C_2S (852 & 975 cm^{-1}), were demonstrated for the three w/s ratio samples. In the first 5 min of the hydration reaction, the raw material Raman peak of C_2S dominates in the three hydration ratio samples. It is noteworthy that the $\nu4$ internal modes of the SiO_4^{4-} chemical bond was also found at the beginning of the hydration reaction [42,44]. As the hydration reaction proceeded to 1 h, weak C–S–H Raman spectra were formed at 655 cm^{-1} for 0.5 and 0.55 hydration ratios. C–S–H was first observed with the 0.6 w/s sample between 1 and 2 h. The intensity of the C–S–H Raman spectra gradually increased as the hydration reaction proceeded for one day. However, unlike C_3S at the same hydration period, barely CH was formed at 356 cm^{-1} for all three C_2S samples. This phenomenon indicates that the C–S–H was formed as the main product by the C_2S hydration reaction due to the lower hydration kinetics. As the hydration reaction proceeded for 14 days, the C_2S sample with w/s ratio of 0.5 showed a slow reaction rate due to the slow increase in the Raman intensity of the C–S–H product. In contrast, the C_2S samples with 0.55 and 0.6 w/s ratios did not show any reduction trend in the hydration reaction. When the hydration reaction proceeds for 28 days, the C_2S sample with w/s ratio of 0.5 already appears to be characterized near the end of the hydration reaction. The 0.55 w/s C_2S started to show a trend of a slower rate of hydration reaction. However, the 0.6 w/s C_2S sample continued to show a trend of continued hydration.

The progress of the hydration reaction could be initially inferred from the Raman spectra by the 60-day long-period examination of the C_2S samples with three hydration ratios. To further understand the correlation between the hydration products and the Raman spectra of C_2S samples, the Raman spectra of 550–950 cm^{-1} were selected for detailed analysis, as shown in Fig. 11. Fig. 11 (a) and (b) show that samples with 0.5 w/s gradually enter the late stage of hydration reaction between 14 and 21 days of hydration reaction; samples with 0.55 w/s enter the late stage of hydration reaction between 21 and 28 days. The C_2S sample with 0.6 w/s showed a slow hydration rate at 28 days of hydration reaction, as shown in Fig. 11 (c).

The Raman characteristic peak intensity ratios of C–S–H at 655 cm^{-1} and C_2S at 852 cm^{-1} were further analyzed, as shown in Fig. 12. Three exponential functions were applied to perform the curving fitting for all three datasets. The minimum value of R square of 0.992 ensured the accuracy of the curve fitting calculation. During the first five days of the hydration reaction, the Raman peak intensity ratio of the three hydration ratios of C_2S samples was uniform. However, on the seventh day of the hydration reaction, the Raman peak intensity ratios of the three samples showed differently due to the different hydration ratios. As the hydration reaction proceeded, the three curves showed different growth rates, which indicated that the samples with higher hydration ratios would produce more products with the same hydration period but different hydration ratios. Based on the modified Avrami equation (2), three curve functions were applied to all C_2S samples, as shown in Fig. 13. A minimum value of R square of 0.991 was calculated to address the peak fitting uncertainties. A similar phenomenon was observed that the higher water-to-solid ratio has greater reactant consumption and a higher degree of hydration. The C_2S sample analysis revealed coefficient 'M' values of 1.238, 1.253, and 1.283 for the 0.6, 0.55, and 0.5 w/s ratios, respectively. These findings provide valuable insights into the hydration potential of C_2S during the long-term hydration stage, highlighting the influence of the w/s ratio and the early-age degree of hydration, which aligns with established principles of classic cement chemistry. The observed variations in the coefficient 'M' values for the different w/s C_2S samples indicate distinct hydration behaviors. Notably, the lower w/s C_2S sample (0.5 w/s) exhibited the highest coefficient 'M' value of 1.283. This observation suggests that the C_2S sample with a lower w/s ratio possesses a greater hydration potential during the long-term hydration stage. This correlation between the w/s ratio and the coefficient 'M' aligns with the fundamental principles of classic cement chemistry, where a lower early-age degree of hydration is known to contribute to a higher potential for hydration over an extended period. By demonstrating the relationship between the coefficient 'M' values and the w/s ratios of C_2S samples, the findings provide valuable insights into the hydration characteristics of C_2S. These results enhance our understanding of the long-term hydration behavior of C_2S, offering a deeper comprehension of the influence of the w/s ratio on the hydration potential and overall performance of cementitious materials. More investigation will be studied in future research.

The XRD patterns of C_2S were examined at various time points, including the initial state, 12 h, 14 days, 28 days, and 60 days, as illustrated in Fig. 14. The XRD analysis clearly identifies the raw C_2S phase in the initial state. As the hydration reaction progresses, new peaks corresponding to $Ca(OH)_2$ and C–S–H gel emerge, observed notably at the 12-h time point. With the hydration process advancing to

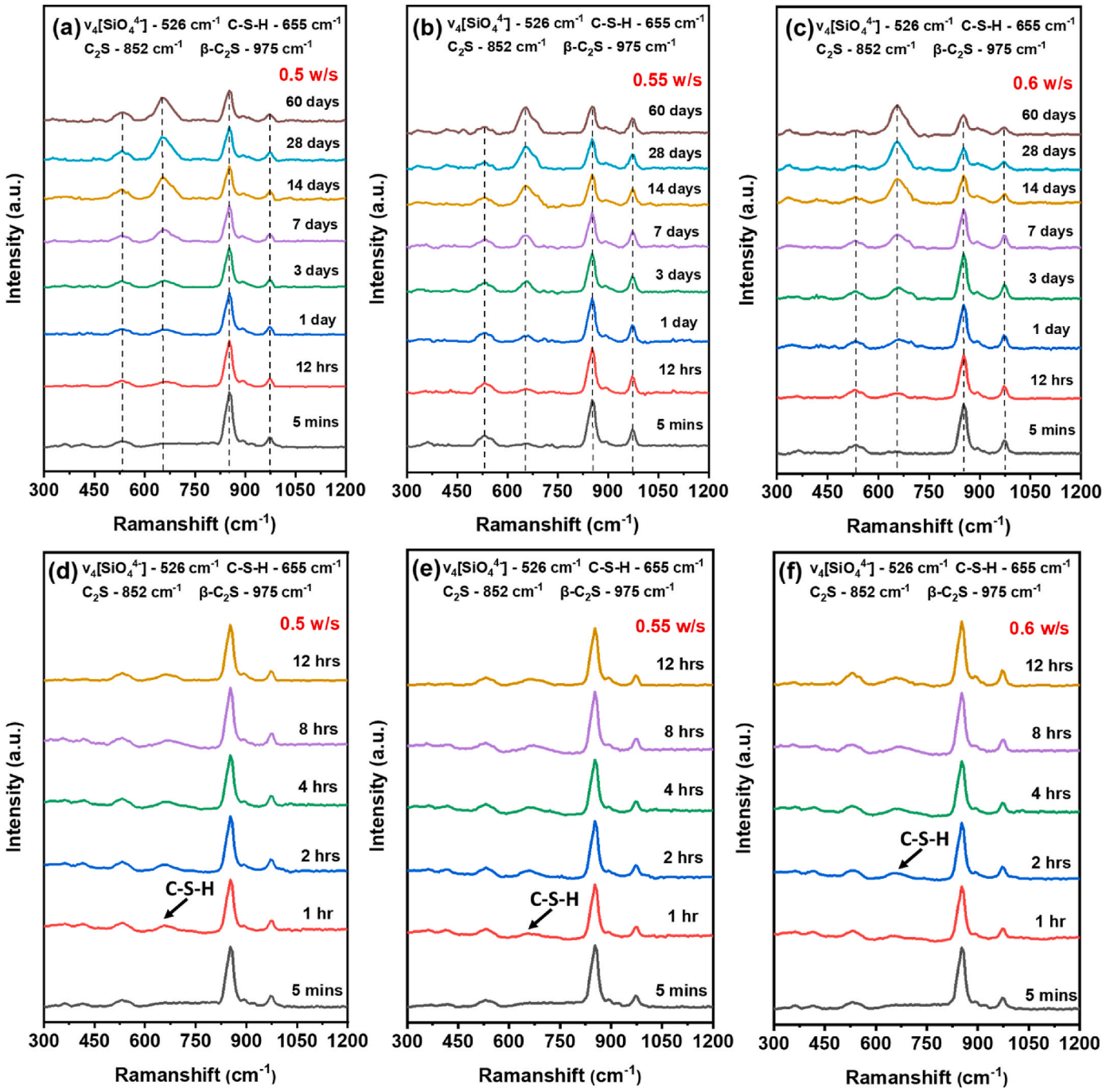

Fig. 10. The Raman spectra of three w/s ratio C_2S paste samples hydration reaction from 5 min to 60 days. Four significant Raman peaks were observed from all three w/s ratio C_2S paste samples. (a) Raman spectra of 0.5 w/s ratio C_2S paste sample hydration reaction in 60 days. (b) Raman spectra of 0.55 w/s ratio C_2S sample hydration reaction in 60 days. (c) Raman spectra of 0.6 w/s ratio C_2S paste sample hydration reaction in 60 days. (d) Raman spectra of 0.5 w/s C_2S sample hydration reaction from 5 min to 12 h. (e) Raman spectra of 0.55 w/s C_2S sample hydration reaction from 5 min to 12 h. (e) Raman spectra of 0.6 w/s C_2S sample hydration reaction from 5 min to 12 h.

14 days, the raw C_2S peak diminishes significantly, while the C–S–H peak becomes dominant in the XRD patterns. The hydrated C_2S samples exhibit a substantial presence of C–S–H and remaining C_2S material. The noticeable decrease in the peaks associated with the C_2S feedstocks after 60 days of hydration indicates the consumption of these silicates during the hydration process, corroborating the earlier findings from Raman spectroscopy. The formation of CH in C_2S hydration is comparatively lower than that in C_3S hydration, making it difficult to discern in the XRD test due to the similar CaO/SiO_2 molar ratio of C_2S to the formed C–S–H gels. Using the TGA analysis method described in the C_3S paste section, the degrees of hydration of the C_2S paste were determined and presented in Fig. 15. As illustrated in the figure, the results obtained from both Raman spectroscopy and TGA demonstrate a generally consistent trend, although slight discrepancies are observed at the initial age (1 day) due to the possible reasons that discussed in the C_3S section.

Concrete monitoring is crucial for assessing the performance, durability, and structural health of concrete structures. *In Situ* fiber-optic Raman probe offers a non-destructive means of evaluating hydration products in concrete, providing real-time monitoring of their formation and development. This technique enables the assessment of hydration

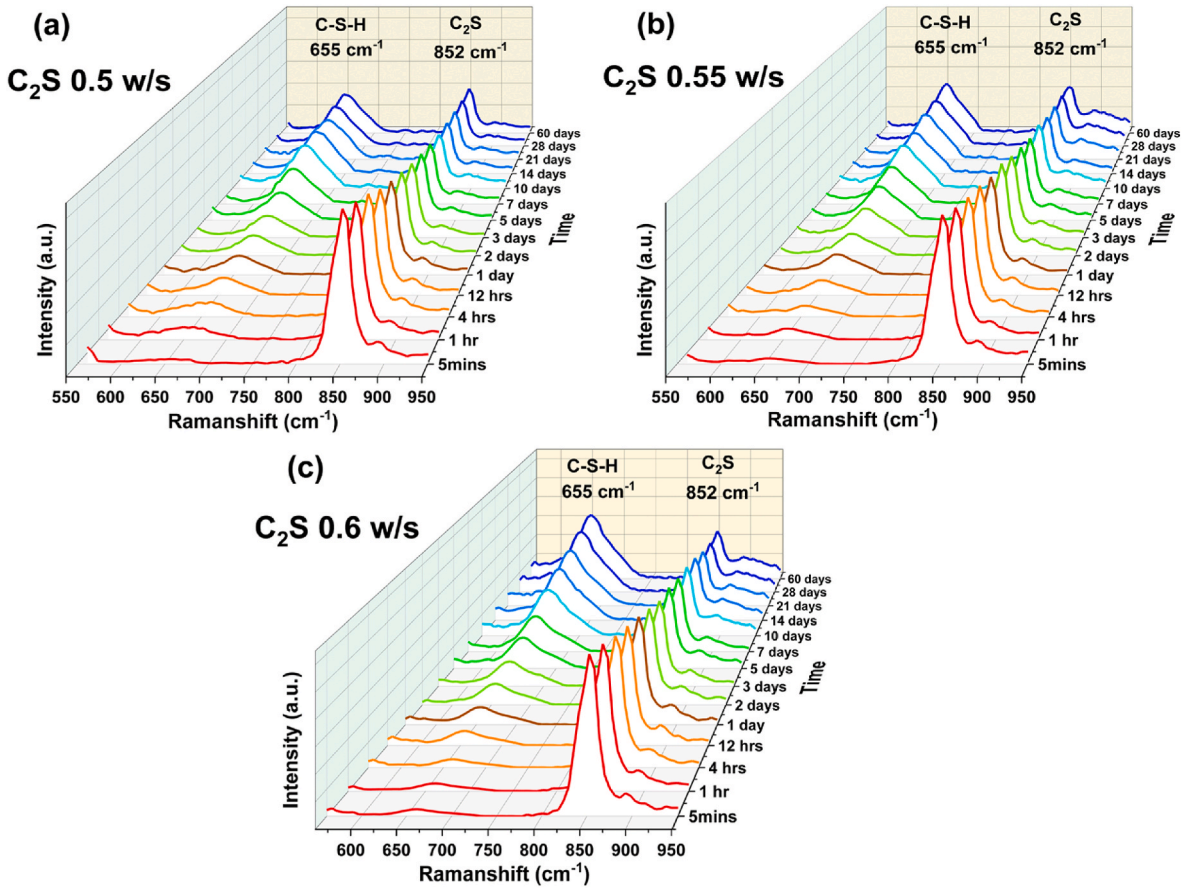

Fig. 11. The 3D Raman spectra of three w/s ratios C_2S samples from 5 min to 60 days hydration reaction in the Raman region between 550 and 950 cm^{-1}. (a) 3D Raman spectra of the 0.5 w/s C_2S hydration sample. (b) 3D Raman spectra of the 0.55 w/s ratio C_2S hydration sample. (c) 3D Raman spectra of the 0.6 w/s ratio C_2S hydration sample. Two significant peaks of C–S–H and C_2S were observed at 655 and 852 cm^{-1} in all three samples with different w/s ratios.

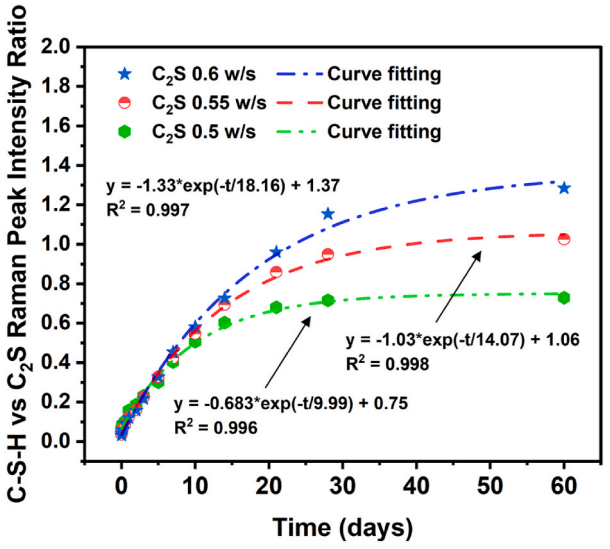

Fig. 12. The relative Raman peak ratio of C–S–H and C_2S as a function of time. The blue dot represents the 0.6 w/s C_2S hydration sample, the red dot represents the 0.55 w/s C_2S hydration sample, and the green dot represents the 0.5 w/s C_2S hydration sample. Three exponential functions were applied for the curve fitting analysis. A minimum 0.996 R square value indicates the curve fitting accuracy. (For interpretation of the references to colour in this figure legend, the reader is referred to the Web version of this article.)

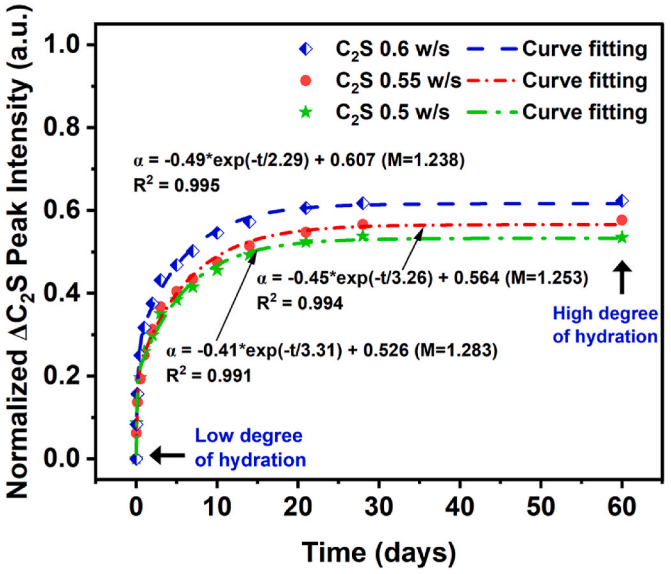

Fig. 13. The consumption (mirrored by variation of Raman peak intensity) of C_2S as a function of time. The blue dot represents the 0.6 w/s C_2S hydration sample, the red dot represents the 0.55 w/s C_2S hydration sample, and the green dot represents the 0.5 w/s C_2S hydration sample. (For interpretation of the references to colour in this figure legend, the reader is referred to the Web version of this article.)

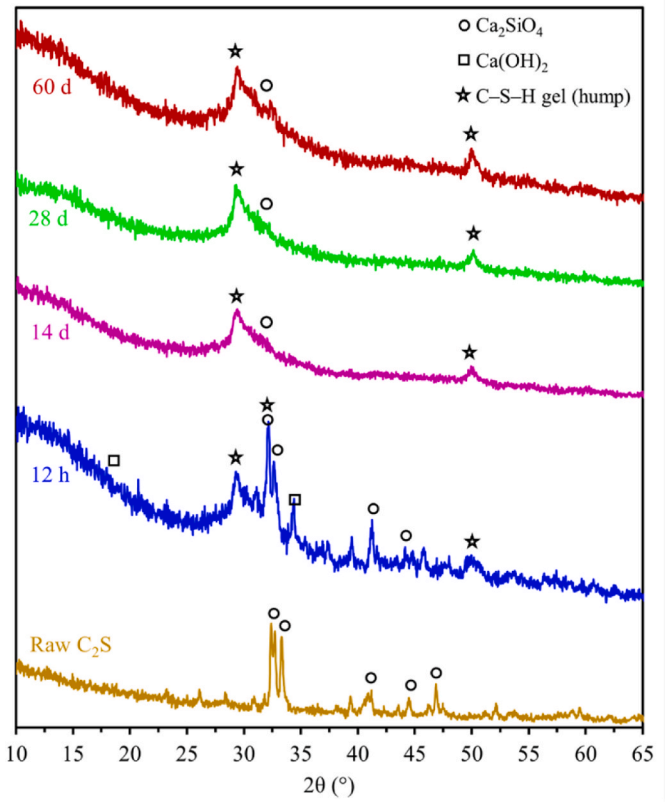

Fig. 14. XRD results of the hydration process of the C_2S sample. XRD patterns illustrate the hydration progress of the C_2S sample at different time intervals, including the raw state, 12 h, 14 days, 28 days, and 60 days.

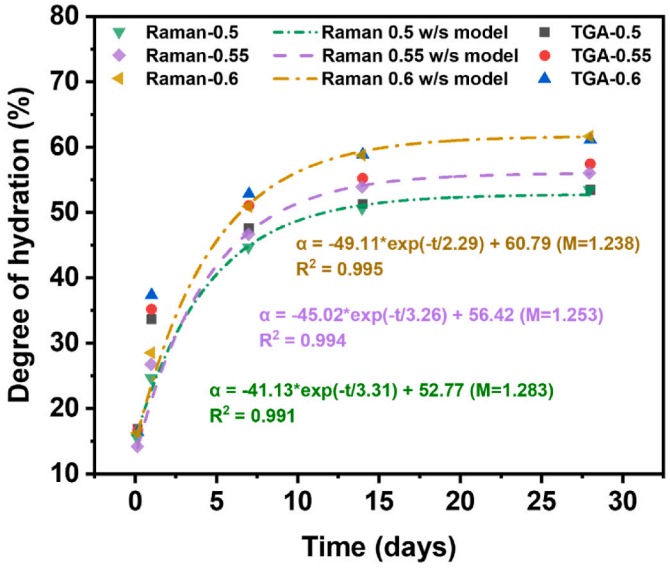

Fig. 15. Degrees of hydration of C_2S paste samples, in comparison with Raman results.

kinetics and the identification of early-stage anomalies or deficiencies in the hydration process. Moreover, the *in situ* fiber-optic Raman probe allows for the quantification of key constituents such as calcium silicates, calcium hydroxide, and calcium silicate hydrates. This quantification aids in evaluating concrete quality and composition, as well as assessing the degree of cement hydration and the utilization of supplementary cementitious materials [55–60]. Additionally, Raman spectroscopy, when applied using fiber-optic probes, is effective in detecting chemical changes and degradation processes in concrete [34–37,61–63]. The fiber-optic Raman probe approach extends this capability to remote or hard-to-reach areas, facilitating continuous monitoring of critical regions vulnerable to chemical attacks, including sulfate or chloride ingress, carbonation, and alkali-silica reaction. The *in situ* monitoring of curing and hardening processes is another application of the fiber-optic Raman probe method. By tracking the evolution of Raman spectra over time, it becomes possible to measure the degree of cement hydration and the development of hydration products. This information can contribute to optimizing curing conditions and predicting concrete strength gain. For long-term structural health monitoring, fiber-optic Raman spectroscopy can be integrated into optical fiber based sensors embedded within concrete structures. This integration enables the detection of internal stresses, strains, and chemical changes over extended periods. By monitoring these parameters, the integrity and performance of the concrete can be assessed, ensuring the long-term durability and safety of the structure.

5. Conclusion

In this study, an *in situ* fiber-optic Raman probe was leveraged to investigate the hydration behavior of cement clinker phases with different w/s ratios. The hydration reactions of C_3S and C_2S, were examined separately under a CO_2-free environment from the beginning to 60 days. The hydration products of C–S–H and CH were well identified over the hydration reaction. XRD and TGA tests substantiated the above results learned from Raman spectroscopy in the known raw materials and post-hydration products. Moreover, thanks to the strong signal and good SNR that made this fiber-optic Raman system unique, the *in situ* fiber-optic Raman probe has successfully traced the evolution of the hydration product, C–S–H, during C_3S and C_2S clinker hydration. The quantitative results revealed the accelerating and decelerating periods of the clinker hydrations. It was also found that C_2S had a slower hydration rate than C_3S, and higher w/s ratios consumed more reactants and gave higher hydration degrees, which were quite consistent with other existing reports. The experimental data had an excellent fit with the well-known slowly evolving theoretical model. Therefore, the *in situ* fiber-optic Raman probe has demonstrated great potential for long-period real-time *in situ* monitoring in future cement chemistry research. In addition, by virtue of the good SNR and the portability of this *in situ* fiber-optic Raman system, it opens a new door for using Raman spectroscopy in future construction fields for on-site monitoring and evaluating the condition and the performance of concrete structures. Towards this long-term goal, the next-step development will be testing the feasibility of monitoring the hydration (homogeneous) and degradation (inhomogeneous) processes of Portland cement. For the latter purpose, multiple fiber-optic Raman probes will be embedded into different depths in cement paste, which is subjected to environmental loads (e.g., sulfate, chloride, and CO_2), so the ingress of harmful ions and their reactions with cement hydrates can be analyzed in a time-resolved manner.

Author contribution

The manuscript was written through contribution of all authors. All authors have given approval for the final version of the manuscript.

Declaration of competing interest

The authors declare that they have no known competing financial interests or personal relationships that could have appeared to influence the work reported in this paper.

Data availability

Data will be made available on request.

Acknowledgement

J.H. is grateful for support from the Roy A. Wilkens Professorship Endowment. Financial support from the National Science Foundation (#1932690) and the Advanced Materials for Sustainable Infrastructure seed funding program at Missouri University of Science and Technology is gratefully acknowledged.

References

[1] K. Scrivener, R. Snellings, B. Lothenbach, A Practical Guide to Microstructural Analysis of Cementitious Materials, CRC Press, Boca Raton, FL, USA, 2016.
[2] W. Liao, X. Sun, A. Kumar, H. Sun, H. Ma, Hydration of binary Portland cement blends containing silica fume: a decoupling method to estimate degrees of hydration and pozzolanic reaction, Frontiers in Materials 6 (2019) 78.
[3] W. Liao, H. Ma, H. Sun, Y. Huang, Y. Wang, Potential large-volume beneficial use of low-grade fly ash in magnesia-phosphate cement based materials, Fuel 209 (2017) 490–497.
[4] J. Bensted, Uses of Raman spectroscopy in cement chemistry, J. Am. Ceram. Soc. 59 (3–4) (1976) 140–143.
[5] C. Tang, T. Ling, K.H. Mo, Raman spectroscopy as a tool to understand the mechanism of concrete durability—a review, Construct. Build. Mater. 268 (2021), 121079.
[6] S.S. Potgieter-Vermaak, J.H. Potgieter, R.V. Grieken, The application of Raman spectrometry to investigate and characterize cement, Part I: a review, Cement Concr. Res. 36 (4) (2006) 656–662.
[7] M. Tarrida, M. Madon, B.L. Rolland, P. Colombet, An in-situ Raman spectroscopy study of the hydration of tricalcium silicate, Adv. Cement Base Mater. 2 (1) (1995) 15–20.
[8] J. Bensted, S.P. Varma, Some applications of infrared and Raman spectroscopy in cement chemistry. Part I-Examination of dicalcium silicate, Cement Technology 5 (1) (1974) 256–257.
[9] L. Black, C. Breen, J. Yarwood, J. Phipps, G. Maitland, In situ Raman analysis of hydrating C3A and C4AF pastes in presence and absence of sulphate, Adv. Appl. Ceram. 105 (4) (2006) 209–216.
[10] M. Conjeaud, H. Boyer, Some possibilities of Raman microprobe in cement chemistry, Cement Concr. Res. (1980) 61–70.
[11] L. Black, C. Breen, J. Yarwood, C. Deng, J. Phipps, G. Maitland, Hydration of tricalcium aluminate (C3A) in the presence and absence of gypsum—studied by Raman spectroscopy and X-ray diffraction, J. Mater. Chem. 16 (13) (2006) 1263–1272.
[12] F. Liu, Z. Sun, C. Qi, Raman spectroscopy of the dehydration process of gypsums, Adv. Cement Res. 27 (8) (2015) 434–446.
[13] T. Schmid, P. Dariz, Shedding light onto the spectra of lime: Raman and luminescence bands of CaO, Ca(OH)2 and CaCO3, J. Raman Spectrosc. 46 (1) (2015) 141–146.
[14] K. Garbev, P. Stemmermann, L. Black, C. Breen, J. Yarwood, B. Gasharova, Structural features of C–S–H (I) and its carbonation in air—a Raman spectroscopic study. Part I: fresh phases, J. Am. Ceram. Soc. 90 (3) (2007) 900–907.
[15] L. Black, C. Breen, J. Yarwood, K. Garbev, P. Stemmermann, B. Gasharova, Structural features of C–S–H (I) and its carbonation in air—a Raman spectroscopic study. Part II: carbonated phases, J. Am. Ceram. Soc. 90 (3) (2007) 908–917.
[16] S.K. Deb, M.H. Manghnani, K. Ross, R.A. Livingston, P.J.M. Monteiro, Raman scattering and X-ray diffraction study of the thermal decomposition of an ettringite-group crystal, Phys. Chem. Miner. 30 (1) (2003) 31–38.
[17] G. Renaudin, R. Segni, D. Mentel, J.-M. Nedelec, F. Leroux, C. Taviot-Gueho, A Raman study of the sulfated cement hydrates: ettringite and monosulfoaluminate, J. Adv. Concr. Technol. (2007) 299–312.
[18] R. Masmoudi, K. Kupwade-Patil, A. Bumajdad, O. Büyüköztürk, In situ Raman studies on cement paste prepared with natural pozzolanic volcanic ash and Ordinary Portland Cement, Construct. Build. Mater. 148 (2017) 444–454.
[19] M. Torres-Carrasco, A.d. Campo, M.A.d. l. Rubia, E. Reyes, A. Moragues, J.F. Fern ández, In situ full view of the Portland cement hydration by confocal Raman microscopy, J. Raman Spectrosc. 50 (5) (2019) 720–730.
[20] R. Tawie, H.-K. Lee, Piezoelectric-based non-destructive monitoring of hydration of reinforced concrete as an indicator of bond development at the steel–concrete interface, Cement Concr. Res. 40 (12) (2010) 1697–1703.
[21] Y.-F. Su, G. Han, A. Amran, T. Nantung, N. Lu, Instantaneous monitoring the early age properties of cementitious materials using PZT-based electromechanical impedance (EMI) technique, Construct. Build. Mater. 225 (2019) 340–347.
[22] G. Han, Y.-F. Su, S. Ma, T. Nantung, N. Lu, In situ rheological properties monitoring of cementitious materials through the Piezoelectric-based Electromechanical Impedance (EMI) Approach, Engineered Science 16 (2021) 259–268.
[23] X. Sun, Y. Du, W. Liao, H. Ma, J. Huang, Measuring the heterogeneity of cement paste by truly distributed optical fiber sensors, Construct. Build. Mater. 225 (2019) 765–771.
[24] W. Liao, Y. Zhuang, C. Zeng, W. Deng, J. Huang, H. Ma, Fiber optic sensors enabled monitoring of thermal curling of concrete pavement slab: temperature, strain and inclination, Measurement 165 (2020), 108203.
[25] C. Zhu, Y. Zhuang, B. Zhang, R. Muhammad, P.P. Wang, J. Huang, A miniaturized optical fiber tip high-temperature sensor based on concave-shaped Fabry–Perot cavity, IEEE Photon. Technol. Lett. 31 (1) (2019) 35–38.
[26] F. Mumtaz, M. Roman, B. Zhang, L.G. Abbas, M.A. Ashraf, Y. Dai, J. Huang, Highly sensitive strain sensor by utilizing a tunable air reflector and the vernier effect, Sensors 22 (19) (2022) 7557.
[27] B. Zhang, R.E. Gerald II, J. Huang, A miniaturized 7-in-1 fiber-optic Raman probe, Opt Lett. 47 (2022) 5561.
[28] E. Cordero, I. Latka, C. Matthäus, I.W. Schie, J. Popp, In-vivo Raman spectroscopy: from basics to applications, J. Biomed. Opt. 23 (7) (2018), 071210.
[29] B. Zhang, H. Tekle, R.J. O'Malley, T. Sander, J.D. Smith, R.E. Gerald, et al., In situ and real-time mold flux analysis using a high-temperature fiber-optic Raman sensor for steel manufacturing applications, J. Lightwave Technol. 41 (2023) 4419–4429.
[30] M.L. Myrick, J. Kolis, E. Parsons, K. Chike, M. Lovelace, W. Scrivens, R. Holliday, M. Williams, In situ fiber-optic Raman spectroscopy of organic chemistry in a supercritical water reactor, J. Raman Spectrosc. 25 (1) (1994) 59–65.
[31] B. Zhang, H. Tekle, R.J. O'Malley, J.D. Smith, R.E. Gerald, J. Huang, In situ high-temperature Raman spectroscopy via a remote fiber-optic Raman probe, IEEE Trans. Instrum. Meas. 72 (2023) 1–8.
[32] J.T. Motz, M. Hunter, L.H. Galindo, J.A. Gardecki, J.R. Kramer, R.R. Dasari, M. S. Feld, Optical fiber probe for biomedical Raman spectroscopy, Appl. Opt. 43 (3) (2004) 542–554.
[33] B. Zhang, M. Asad Rahman, J. Liu, J. Huang, Q. Yang, Real-time detection and analysis of Foodborne pathogens via machine learning based fiber-optic Raman sensor, Measurement 217 (2023) 113121.
[34] Y. Yue, J.J. Wang, P.M. Basheer, J.J. Boland, Y. Bai, Characterisation of carbonated Portland cement paste with optical fibre excitation Raman spectroscopy, Construct. Build. Mater. (2017) 369–376.
[35] Y. Yue, J.J. Wang, P.M. Basheer, J.J. Boland, Y. Bai, A Raman spectroscopy based optical fibre system for detecting carbonation profile of cementitious materials, Sensor. Actuator. B Chem. 257 (2018) 635–649.
[36] Y. Yue, Application of Optical Fibre Raman Spectroscopy for Characterising Carbonation and Chloride Attack of Cementitious Materials, PhD diss, University College London (University of London), 2015.
[37] Y. Yue, Y. Bai, P.M. Basheer, J.J. Boland, J.J. Wang, Monitoring the cementitious materials subjected to sulfate attack with optical fiber excitation Raman spectroscopy, Opt. Eng. 52 (10) (2013), 104107.
[38] Y. Yue, J.J. Wang, P.M. Basheer, Y. Bai, In-situ monitoring of early hydration of clinker and Portland cement with optical fiber excitation Raman spectroscopy, Cement Concr. Compos. 112 (2020), 103664.
[39] B.L. McClain, S.M. Clark, R.L. Gabriel, D. Ben-Amotz, Educational applications of infrared and Raman Spectroscopy: a comparison of experiment and theory, J. Chem. Educ. 77 (5) (2000) 654.
[40] F. Liu, Z. Sun, Feasibility study of using Raman spectroscopy to detect hydration in wet pastes, ACI Mater. J. 110 (6) (2013) 611.
[41] F. Liu, Z. Sun, C. Qi, Raman spectroscopy study on the hydration behaviors of Portland cement pastes during setting, J. Mater. Civ. Eng. 27 (8) (2015), 04014223.
[42] J. Ibáñez, L. Artús, R. Cuscó, Á. López, E. Menéndez, M.C. Andrade, Hydration and carbonation of monoclinic C2S and C3S studied by Raman spectroscopy, J. Raman Spectrosc.: An International Journal for Original Work in all Aspects of Raman Spectroscopy, Including Higher Order Processes, and also Brillouin and Rayleigh Scattering 38 (1) (2007) 61–67.
[43] C. Tang, T. Ling, K.H. Mo, Raman spectroscopy as a tool to understand the mechanism of concrete durability—a review, Construct. Build. Mater. 268 (2021), 121079.
[44] C. Remy, B. Reynard, M. Madon, Raman spectroscopic investigations of dicalcium silicate: polymorphs and high-temperature phase transformations, J. Am. Ceram. Soc. 80 (2) (1997) 413–423.
[45] Y. Gogotsi, C. Baek, E. Kirscht, Raman microspectroscopy study of processing-induced phase transformations and residual stress in silicon, Semicond. Sci. Technol. 14 (10) (1999) 936.
[46] P. Li, W. Li, K. Wang, J.L. Zhou, A. Castel, S. Zhang, et al., Hydration of Portland cement with seawater toward concrete sustainability: Phase evolution and thermodynamic modelling, Cement Concr. Compos. 138 (2023) 105007.
[47] P. Li, W. Li, T. Yu, F. Qu, V.W.Y. Tam, Investigation on early-age hydration, mechanical properties and microstructure of seawater sea sand cement mortar, Construct. Build. Mater. 249 (2020) 118776.
[48] P. Li, W. Li, Z. Sun, L. Shen, D. Sheng, Development of sustainable concrete incorporating seawater: A critical review on cement hydration, microstructure and mechanical strength, Cement Concr. Compos. 121 (2021) 104100.
[49] F. Qu, W. Li, K. Wang, V.W.Y. Tam, S. Zhang, Effects of seawater and undesalted sea sand on the hydration products, mechanical properties and microstructures of Cement Mortar, Cement Concr. Compos. 310 (2021) 125229.
[50] M. Avrami, Kinetics of phase change. I General theory, J. Chem. Phys. 7 (12) (1939) 1103–1112.
[51] J. William, R. Mehl, Reaction kinetics in processes of nucleation and growth, Trans. Metall. Soc. AIME 135 (1939) 416–442.
[52] S. Garrault, A. Nonat, Hydrated layer formation on tricalcium and dicalcium silicate surfaces: experimental study and numerical simulations, Langmuir 17 (26) (2001) 8131–8138.

[53] J.J. Thomas, A new approach to modeling the nucleation and growth kinetics of tricalcium silicate hydration, J. Am. Ceram. Soc. 90 (10) (2007) 3282–3288.
[54] J.J. Thomas, J.J. Biernacki, J.W. Bullard, S. Bishnoi, J.S. Dolado, G.W. Scherer, A. Luttge, Modeling and simulation of cement hydration kinetics and microstructure development, Cement Concr. Res. 41 (12) (2011) 1257–1278.
[55] Y. Yue, J.J. Wang, P.A. Basheer, Y. Bai, Establishing the carbonation profile with Raman spectroscopy: effects of fly ash and ground granulated blast furnace slag, Materials 14 (7) (2021) 1798.
[56] N. Garg, K. Wang, S.W. Martin, A Raman spectroscopic study of the evolution of sulfates and hydroxides in cement–fly ash pastes, Cement Concr. Res. 53 (2013) 91–103.
[57] S.S. Potgieter-Vermaak, J.H. Potgieter, M. Belleil, F. DeWeerdt, R.V. Grieken, The application of Raman spectrometry to the investigation of cement: Part II: a micro-Raman study of OPC, slag and fly ash, Cement Concr. Res. 36 (4) (2006) 663–670.
[58] Y. Yue, J.J. Wang, Y. Bai, Tracing the status of silica fume in cementitious materials with Raman microscope, Construct. Build. Mater. 159 (2018) 610–616.
[59] S. Martínez-Ramírez, M. Frias, Micro-Raman study of stable and metastable phases in metakaolin/Ca(OH)2 system cured at 60 °C, Appl. Clay Sci. 51 (3) (2011) 283–286.
[60] M. Frías, S. Martínez-Ramírez, Use of micro-Raman spectroscopy to study reaction kinetics in blended white cement pastes containing metakaolin, J. Raman Spectrosc.: An International Journal for Original Work in all Aspects of Raman Spectroscopy, Including Higher Order Processes, and also Brillouin and Rayleigh Scattering 40 (12) (2009) 2063–2068.
[61] K.N. Jallad, M. Santhanam, M.D. Cohen, D. Ben-Amotz, Chemical mapping of thaumasite formed in sulfate-attacked cement mortar using near-infrared Raman imaging microscopy, Cement Concr. Res. 31 (6) (2001) 953–958.
[62] C. Balachandran, J.F. Muñoz, T. Arnold, Characterization of alkali silica reaction gels using Raman spectroscopy, Cement Concr. Res. 92 (2017) 66–74.
[63] T. Ling, C. Balachandran, J.F. Munoz, J. Youtcheff, Chemical evolution of alkali–silicate reaction (ASR) products: a Raman spectroscopic investigation, Mater. Struct. 51 (1) (2018) 1–9.